RSC Advances

ROYAL SOCIETY OF CHEMISTRY

www.rsc.org/advances

Nitrogen- and oxygen-containing activated carbons from sucrose for electrochemical supercapacitor application

Navaladian Subramanian and Balasubramanian Viswanathan*

National Center for Catalysis Research (NCCR),
Indian Institute of Technology Madras,
Chennai 600 036, India.
E-mail: bvnathan@iitm.ac.in
Tel: +91 44 2257 4241

Abstract

Nitrogen- and oxygen-containing activated carbons have been synthesized from sucrose and ammonium nitrate (AN) by carbonization at different temperatures (600 - 900 °C) under a flow of nitrogen gas with steam. A set of carbons have been synthesized without AN. The carbons have been characterized by using X-ray diffractometry (XRD), elemental analysis, solid-state ^{13}carbon nuclear magnetic resonance (NMR) spectroscopy, X-ray photoelectron spectroscopy (XPS), thermo-gravimetric analysis (TGA), di-nitrogen adsorption-desorption, Fourier transform infrared (FTIR) spectroscopy, scanning electron microscopy (SEM) and transmission electron microscopy (TEM) techniques. Nitrogen from AN has been found to be incorporated into carbon samples. Electrochemical performances of the carbons have been studied in 1 M sulphuric acid using cyclic voltammetry and galvanostatic charge-discharge cycling. The use of AN favors the formation of carbons with higher surface areas and graphitic nature. One of the carbons with a BET surface area of 518 m^2 g^{-1}, a nitrogen content of 3 % and an oxygen content of 20.4 % shows a specific capacitance of 277 F g^{-1}. Carbons obtained using AN show better capacitance than the ones obtained without AN. Higher carbonization temperatures favor the formation of carbon with the higher capacitance values.

Keywords: Nitrogen-containing carbon; activated carbon; sucrose; ammonium nitrate; steam activation; supercapacitor

* Corresponding author e-mail: bvnathan@iitm.ac.in

1. Introduction

In recent years, supercapacitor has become one of the most important charge storage devices with the advantages of exhibiting high power density (10 $kW \cdot kg^{-1}$), high charge/recharge rate (seconds) and long cycle life (>10^5).[1, 2] There are two types of capacitance known thus far and those are electric double layer capacitance (EDLC) involving the charge storage by simple electrostatic attraction between surface of the charged electrode and electrolyte ions, a non-faradaic process, and pseudocapacitance involving the fast and reversible reduction or oxidation, a faradaic process, of the bulk or surface of electrode.[3, 4] In general, carbon materials are known to exhibit EDLC characteristics as they show fairly good electric conductivity, inertness, high surface area and suitable porosity.[5] Nevertheless, the presence of certain oxidizable/reducible functional groups in carbon is responsible for it to show pseudocapacitance characteristics besides EDLC.[6] Carbon materials are suitable candidates for capacitor applications due to the abundance, significant to high electrical conductivity, chemical (both in acid and alkali) and electrochemical (high operational window of potential) stabilities and light weight due to the low atomic weight of 12 (to show high gravimetric capacity). [5, 7] Among different types of carbons known, activated carbons have advantages such as low cost, higher surface area and tunability of their pore sizes by activation processes. Moreover, in the case of composite electrodes based on metal oxide or conducting polymer with activated carbons, activated carbons are used as conductive-additive for improving the rate performance or as matrix for improving cycling ability by buffering volume changes, respectively.[7] The activation processes employed to improve the surface areas and pore sizes of carbons are classified into chemical and physical activations. The chemical activation process deals with the use of main activating agents such as KOH, $ZnCl_2$ and H_3PO_4 whereas physical activation deals with mainly the use of activating agents such as steam, CO_2 and air.[8] Although the chemical activation leads to higher surface area, the residues (ash) left behind in the resulting carbon demand tedious post-synthesis work-ups. In contrast, steam activation does not

cause the incorporation of any residues into carbon, except for oxygen, so post-synthesis cleaning is not necessary in this case.

Sucrose is one of the carbon sources, because it, being a carbohydrate, can be carbonized by dehydration to get carbon in a facile manner.[9] Carbons obtained from sucrose are free from impurities and inexpensive.[10] Presence of nitrogen and oxygen in the lattice or nitrogen- and oxygen-based functional groups in carbon shows many advantages such as enhanced conductivity[11], offering pseudocapacitance[5, 12] and increased wettability towards aqueous electrolytes.[5] In order to make a N-containing carbon, N-containing precursors such as melamine-formaldehyde,[13] polypyrrole, polyaniline [14] or waste coffee [15] have been carbonized, carbon has been impregnated with the N-containing compounds such as melamine or urea before a heat-treatment [16], or using NH_3 [17] or NH_3-air mixture (for ammoxidation) during carbonization.[7, 18] Incorporation of oxygen in the carbon materials is performed by using O-containing precursors such as sucrose,[19] activation with steam, KOH or air,[8] treatment with HNO_3,[20] oxygen plasma[21] or electro-oxidation.[22] A combustion method dealing with synthetizing nanoparticles of different oxides using sucrose as the fuel, polyvinyl alcohol (PVA) as matrix and nitrate salt of the metal or non-metal, whose oxide is of interest, as the combusting agent has been reported.[19] Upon evaporation of water from the mixture, formation of a fluffy material was observed, which later was heated in air atmosphere to obtain nanoparticles of the metal oxide by removing the carbonaceous matters from sucrose and other impurities. Herein, we report the synthesis of activated carbons using sucrose as the carbon source and fuel and ammonium nitrate as the combusting agent and nitrogen source. The fluffy material obtained was carbonized under the flow of nitrogen gas with steam to obtain activated carbons. For the best of authors' knowledge, synthesis of nitrogen (N)-containing carbon from the mixture of sucrose and ammonium nitrate has not been reported yet. Ammonium nitrate is used here, because it decomposes completely into gaseous products at temperatures as low as 210 °C.[23] So, the unreacted ammonium nitrate can be removed easily during the carbonization process.

2. Experimental section

2.1 Methods

2.1.1. Synthesis of activated carbons

In a typical synthesis, 15 g of sucrose ($C_{12}H_{22}O_{12}$) and 5 g of ammonium nitrate (NH_4NO_3) (AN) were dissolved in 80 ml volume of DI water and aged in an air oven at 120 °C for 24 h. A fluffy material was observed and it was carbonized in a horizontal tubular furnace using a quartz boat at temperatures, viz., 600, 700, 800, and 900 °C, for 6 h in a stream of nitrogen gas containing water vapors. Nitrogen gas was passed through a water bubbler (cylindrical; 120 mL volume; 50 % filled with DI H_2O) at 29 °C at a flow rate of 50 ml min^{-1}. Heating ramp of the furnace was 25 °C min^{-1}. After carbonization, samples were naturally cooled to room temperature under nitrogen gas flow. Another set of samples with 2:1 wt. ratio of sucrose and AN was synthesized. For comparison, a set of carbon samples was synthesized from sucrose in the absence of AN under the similar conditions. In this case, no fluffy but a hard and pasty stuff was observed. The carbon samples synthesized using 3:1 and 2:1 wt. ratios of sucrose and AN are denoted as 'CN_A' and 'CN_B'. Carbons obtained from sucrose alone are marked as 'C'. Temperature (in °C) of the carbonization is suffixed with the code of sample without unit. The as-synthesized samples were ground well with a mortar-pestle before characterization.

2.2 Characterization

Powder X-ray diffraction (XRD) patterns of the carbon samples were recorded using Rigaku MiniFlex2 diffractometer at a scan rate of 0.1° s^{-1} with Ni-filtered Cu K_α radiation (λ =1.5406 Å) as the X-ray source. CHN elemental analyses of the samples were carried out with a Perkin-Elmer 2400 II series CHNS/O analyzer. Solid-state ^{13}C NMR studies were carried out using a Bruker Avance™ 400 MHz instrument of probe head with a zirconium rotor of 4 mm diameter. The entire spectrum was recorded at a spinning speed of 12 kHz. X-ray photoelectron spectra (XPS) were recorded using an Omicron NanoTechnology instrument with Mg Kα

radiation. The base pressure of the analysis chamber during the scan was 2×10^{-10} mbar. The spectra were recorded with a step width of 0.05 eV. The pass energies for individual and survey scans were 20 and 100 eV, respectively. Data were processed using the CasaXPS program (Casa Software Ltd., UK). Thermo-gravimetric analysis (TGA) was performed with Perkin-Elmer TGA (Delta series TGA7) instrument at a heating rate of 10 °C min^{-1} in air atmosphere. Nitrogen adsorption-desorption experiments were carried out at -196 °C using a Carlo-Erba Sorptomatic (model 1990) sorpometer and a Micrometrics ASAP 2010 accelerated surface area systems after degassing samples at 150 °C for 12 h. Specific surface areas of the samples were determined based on the Brunauer-Emmett-Teller (BET) method. The total pore volume was calculated from the amount of nitrogen adsorbed at a relative pressure of $P/P_0 = 0.99$. Micropore and mesopore size distributions were calculated by Horvath-Kawazoe (HK) and Barrett-Joyner-Halenda (BJH) methods respectively. FTIR spectra of the samples were recorded using Perkin-Elmer spectrum 1 instrument in the range 400-4000 cm^{-1} at room temperature. The powdered samples were ground with KBr and pressed into pellets for recording the FTIR spectra. Scanning electron micrographs were recorded using FEI Quanta FEG 200 scanning electron microscope working at 30 kV. Transmission electron micrographs (TEM) were collected using a Philips CM12 microscope operating at 100 kV accelerating voltage. Sample for TEM imaging was prepared by dispersing the sample in ethanol by sonication followed by drop-drying on copper grids coated with carbon film.

2.3. Electrode fabrication and electrochemical measurements

Electrochemical performance of carbon samples was studied using cyclic voltammetry curves and charge-discharge cycling. Fabrication of electrodes for electrochemical studies was done as follows. In a typical procedure, 10 mg of carbon samples was dispersed in 0.25 ml of doubly distilled water in a vial by ultrasonication. From the colloid, a volume of 10 µl was transferred on to polished glassy carbon surface, dried at 60 °C to get the semisolid and 5 µl of

Nafion solution (5 wt.% in lower aliphatic alcohol and water) was coated on the sample as the binder.[24] Electrochemical studies were performed in 50 ml of 1 M sulphuric acid solution. Cyclic voltammograms were recorded at a scan rate of 10 mV s^{-1} in the potential window of 0 to 1 V (vs Ag/AgCl) and galvanostatic charge-discharge curves were collected with a current of 0.5 mA. Cyclic voltammetric and galvanostatic charge-discharge experiments were carried out using a CHI 660A (CH Instruments, USA) electrochemical work station. For the electrochemical studies, a conventional three-electrode cell composing a polished glassy carbon (GC) (0.07 cm^2) working electrode, a Ag/AgCl (Satd. KCl) reference electrode and a Pt foil (5 cm^2) counter electrode was used. Nitrogen gas was purged through the electrolyte solution for removing dissolved oxygen before and during the electrochemical measurements.

3. Results and Discussion

3.1. Yields and elemental analysis of carbons

A photograph of precursors corresponding to C and CN_B samples is shown in Fig. 1. It is clear that formation of fluffy materials is observed only in the case of using NH_4NO_3 with sucrose due to the combustion that occurs. The fluffy material forms due to the sudden evolution of gases, taking place due to combustion. The precursor from sucrose alone is highly sticky whereas the fluffy material is crispy and deliquescent. It was observed that higher the AN content, the higher would be the volume of fluffy material. The yields of the synthesized carbons are provided in Table 1. The C samples show the highest yield of 84.2 % and increase in the temperature of synthesis consistently reduces the yield. CN_A and CN_B samples show lower yields than C samples. Between CN_A and CN_B samples, CN_A analogues show higher yield than CN_B. The loss of carbon is expected to take place due to the decomposition of sucrose, the precursor, during the initial treatment with AN and during the carbonization at higher temperatures, and burning-off of the carbon occurring due to steam activation. The lower yields shown by CN_A and CN_B are due to the loss of carbon into escaping gaseous products, which in turn due to the high degree of decomposition of precursor.

C, H, N and O elemental composition of the carbon samples are given in Table 1. The oxygen content (wt %) of the carbon samples have been calculated by subtracting the sum wt % of C, H and N elements from hundred. The C, H and O content of sucrose is 42.11, 6.43 and 51.46 respectively. The carbon content of the synthesized samples range from 73.5 to 80.1 %. This implies that carbon content has increased due to the carbonization at the expense of hydrogen and oxygen (i.e., dehydration). Hydrogen content of the carbon samples ranges from 2 to 3.7 %. Hydrogen content of C samples is found to be higher than that of CN_A and CN_B samples, implying that the combustion might be reason for the observed high degree of hydrogen removal and/or that C sample might have smaller and more polynuclear aromatic hydrocarbons (PAHs). Also, presence of lower content of H indicates the presence of bigger and lesser condensed polynuclear aromatic hydrocarbons in carbon because H content arises mainly from the periphery of the PAHs.[25] Presence of nitrogen in the carbons (CN_A and CN_B) obtained *via* combustion route by using AN is evidenced. And, it is notable that C samples are nitrogen-free. These observations reveal that nitrogen in CN_A and CN_B is from AN that was used as the combustion agent, but not from the nitrogen gas stream used for carbonization. Although the N content is as high as 8.8 % in the case of CN_B600, it is only 3 % for CN_B900. This observation indicates that amount of nitrogen incorporated in the carbon decrease when the temperature of carbonization increases. Oxygen content of the carbons is in the range of 12.1 to 22.8 %. Except for C samples, O content of the carbons is found to increase with the increase in the carbonization temperature. This increase might be due to degree of reactivity between steam and carbon, which probably increases with the raise in the temperature from 600 °C to 900 °C.

3.2. Powder XRD studies

XRD powder patterns of C, CN_A and CN_B samples obtained at different temperatures are given in Fig. 2. The broad peaks in the 2θ range of 22.7° to 25.5° and 43.7° to 43.8° respectively correspond to the (002) planes and (101) planes of amorphous carbon with hexagonal phase

(JCPDS file no 41-1487) [26]. The inter planar distances, d , of (002) peaks correspond to inter layers(graphene) distance of carbon and are provided in Table 1.[26] The $d_{(002)}$ of graphite is 3.35 Å and the $d_{(002)}$ values of the synthesized carbons deviate from that of graphite by different magnitudes. For the set of C, CN_A and CN_B samples, the minimum $d_{(002)}$ value are 3.71, 3.54 and 3.50 Å respectively. This observation reveals that CN_A and CN_B samples show $d_{(002)}$ value closer to that of graphite, meaning CN_A and CN_B samples are more graphitic than C samples. Moreover, increase in the carbonization temperature shrinks the inter layer distance ($d_{(002)}$) or increases the degree of graphitization in all samples. Average crystallite size, L_c, of carbons calculated using Scherer's equation from XRD peaks corresponding to (002) planes is attributed to the size of the crystallites along the 'c' axis of the hexagonal lattice and given in Table 1. The Scherer's equation used for the calculation is $L_c = 0.89\lambda/\beta\cos\theta$, where, ' λ' is wavelength of X-rays, 'β' is full width at the half maximum of a diffraction peak and 'θ' is Bragg angle of the peak.[27] The highest L_c shown by C samples is found to be 7.42 Å, which is lower than that of CN_A (9.38 Å) and CN_B (9.72 Å) samples. Calculation of L_a using (10) peak has not been done due to that (10) peaks of carbons studied here are too small and also merged with that of (101) peaks. Average number of layers 'N_c' of carbons along the 'c' axis of their hexagonal lattice is calculated by dividing their L_c value by their $d_{(002)}$ value and given in Table 1. The N_c values show that highest N_c of C samples is 2 while those of CN_A and CN_B are 2.61 and 2.78 respectively. This implies that CN_A and CN_B samples possess more carbon layers in 'c' axis.[28] These observations imply that the combustion route followed to synthesize carbon samples might be responsible for the lower d values and the higher L_c of the CN_A and CN_B carbons.

3.3. ^{13}C NMR and FT-IR studies

In order to understand the changes in the nature of carbons present in the synthesized carbon samples, solid-state ^{13}C NMR spectra of sucrose, fluffy material of CN_A and carbon samples synthesized at 800 °C were recorded, and the spectra are provided in Fig. 3. The six peaks

observed for sucrose are in the range of 63 - 106 ppm, which correspond to the aliphatic carbons of carbohydrates.[29-31] The intense peak centered at 76 ppm corresponds to hydroxylated methylene carbon.[29] Moving onto the fluffy material, a single broad peak centered at 76 ppm is observed, corresponding to hydroxylated methylene carbon as in the case of sucrose. However, merging of six peaks to a single peak has taken place during the treatment of sucrose with AN, indicating that the nature of sucrose has changed due to its reaction with AN. In the case of C800, there are three predominant peaks seen and their positions are at 124, 158 and 198 ppm. And, the peak at 124 ppm indicates the presence of the sp^2 carbon which corresponds to polynuclear aromatic hydrocarbons or graphite-like carbon while the one at 158 ppm belongs to the aromatic carbon with oxygen functionalities such as hydroxyl (phenolic). The peak present at 198 ppm corresponds to aromatic carbon attached to carbonyl carbons such as aldehyde and ketones.[31] The peak at 158 ppm is more intense, indicating that phenolic carbon is present in higher amount than normal aromatic carbon and also that more of oxygen functionalities is present in C800. As for CN_A800 and CN_B800, only the broad single peaks centered respectively at 127 ppm and 131 ppm are observed. These peaks are attributed to the graphite-like carbons. Thus, ^{13}C NMR spectral studies show that aliphatic carbons from sucrose or fluffy materials are converted into graphite-like aromatic carbons.

FTIR spectra of sucrose, fluffy material of C, CN_A, and CN_B carbons are given in Fig. 4. Sucrose shows the absorption bands at 3385, 2948, and 1434 cm^{-1}, corresponding to O-H stretching, C-H stretching and CH_2 scissoring vibrations respectively. And, peaks observed at 1060 and 991cm^{-1} are attributed to C-O stretching and deformation vibrations respectively. The band at 572 cm^{-1} is due to C-O-C deformation vibrations.[32, 33] C600 shows a weak band for O-H stretching along with C-H stretching vibration in addition to weak bands located at 1718 cm^{-1}, which corresponds to C=O vibrations. The band at 1585 cm^{-1} is probably a collective band that is contributed by the aromatic ring mode, conjugated systems such as ketoester, diketone, and carboxylate structures.[34] The broad band observed between 1500 and 1060 cm^{-1} is owing to C-O

stretching and O-H bending (in-plane) vibrations. The weak bands observed at 878 and 800 cm^{-1} are due to C-H bending vibrations.[35, 36] Strong and more intense bands observed for sucrose become weak while moving on to carbons due to the formation of the rigid, extended network of carbon from the molecular species, i.e., sucrose. This observation confirms that, during carbonization, aromatic C=C bond is generated from aliphatic carbons of sucrose and that removal O-H groups have occurred by dehydration. On increase in the carbonization temperature to 800 and 900 °C, C-H bonds disappear and free O-H groups are generated as evidenced by the weak bands seen at 3835 and 3740 cm^{-1}.[37]

Moving onto the fluffy material, a pair of new bands is observed at 1712 and 1630 cm^{-1}. These bands might be because of C=O stretching vibrations and these carbonyl functional groups might have been created due to the oxidation of sucrose, which probably takes place due to the combustion. However, bands pertaining to C=O stretching are absent in the case of CN_A600, implying that carbonyl groups are removed during carbonization process at 600 °C or the peak shifted to low frequencies due to the formation of extended carbon network. The tiny bands observed below 900 cm^{-1} are probably due to O-H bending (out-of-plane) and C-H bending vibrations. As for CN_A700, a small band at 1566 cm^{-1} is probably a collective band that is contributed by the aromatic ring mode, conjugated systems such as ketoester, diketone, and carboxylate structures.[34] The band covering 1450 to 1000 cm^{-1} corresponding to C-O stretching as in ether or phenol.[38, 39] Possibility of phenolic C-O bond is low or ruled out due to the absence O-H band in the IR spectra. Further increase of carbonization temperature to 800 and 900 °C has caused C=C stretching vibration to shift bathochromically to 1534 and 1542 cm^{-1} respectively. The rationale for these shifts is that extension of carbon network (i.e., increase in conjugation) might have occurred due to the carbonization performed at higher temperatures. On the other hand, CN_B600 shows the only bands of aromatic ring (C=C) of conjugated systems with ketoester, diketone, and carboxylate structures and C-O stretching, implying that, as compared to

C and CN_A analogues, CN_B samples underwent a higher degree of carbonization.[34] This higher degree of carbonization shown by CN_B is probably due to the use of more AN. So, there are definite differences between the carbons obtained with and without the use of AN. There is a possibility that some C=N stretching bands might be present in the spectra of CN_A and CN_B but they might have been merged with aromatic ring (C=C) stretching bands, as the content of N is evidenced by CHNO and XPS results.

3.4. XPS analysis

In order to understand the chemical state of carbon, oxygen and nitrogen elements, XPS were recorded for C900 and CN_B900 samples and the results are presented in Fig. 5. The C1s spectra of C900 show a peak which is resolvable by deconvolution into 3 peaks, namely, C-I, C-II and C-III, with the binding energy values of 284.7, 286.4 and 287.5 eV and with the peak areas (%) of 54.1, 33 and 12.9, respectively. The peak C-I corresponds to graphitic carbon while C-II corresponds to carbon in phenol, and/or ether groups.[22, 40-43] And, the peak C-III is attributed to carbonyl and/or quinone functionalities. In the case of C900, there was no peak observed for nitrogen in the N1s region (data not given). The resolved O1s spectra of C900 shows two peaks (O-II and O-III) centered at 533.3 and 535.7 eV with the peak areas of 91.1 and 8.9 %, respectively. The peak O-II is due to oxygen in phenol, and/or in ether while the peak O-III is due to chemisorbed oxygen (carboxylic group) and/or water, respectively.[20, 34, 40, 42, 44, 45]

The C1s spectrum of CN_B900 exhibit three resolved peaks (C-I, C-II and C-III), centered at 284.5, 285.9 and 287.5 eV respectively. The percentages of relative peak areas are 68.2, 22.4 and 9.4. Similar to C900, C-I is attributed to graphitic, C-II is attributed to phenolic, and/or ether groups and C-III peak is attributed to carbonyl and/or quinone functionalities.[22, 40-43] It is interesting to note that the relative area of graphitic carbon is higher for CN_B900 (68.2 %) than C900 (54.1 %). The N1s spectrum shows two resolved peaks located at 398.6 (area: 33.7 %) and 400.9 eV (area: 66.3 %), corresponding to pyridinic (N-6) and quaternary (N-Q) nitrogens

respectively.[12, 20, 34, 43] As there is nitrogen in the sample, C-N bond might have also contributed to peaks C-II and C-III in C1s spectrum of CN_B900.[46-48] The N1s spectra imply that N atom has substituted some C atoms in the carbon lattice. The O1s spectrum of CN_B900 yields the three resolved peaks (O-I, O-II and O-III) positioned at 531.3, 533 and 535.8 eV with the relative peak areas of 45.9, 47 and 7.1 % respectively. The peaks O-I is indexed to quinonic and/or carbonyl oxygen and O-II is indexed to oxygens in phenol and/or ether. And, O-III corresponds to chemisorbed oxygen (carboxylic group) and/or water, respectively.[36, 39, 41-44]

3.5. BET surface area and TG-DTG analyses

BET surface areas and total pore volumes of the carbon samples are given in Table 1. All the three sets of carbon samples show increase in the surface area with the increase in the carbonization temperature. This increase of surface area is due to the generation of new pores which is, in turn, due to the burning off of the carbon occurring by the reaction of carbon with steam.[49] High temperatures are found to be effective to burn carbon so that more pores are created. In the current work, sintering and burning of carbon take place simultaneously because the carbonization and the activation are performed simultaneously. The C samples show surface area values in the range of 11-205 $m^2 g^{-1}$. On the other hand, CN_A samples show higher surface area values, ranging from 105-489 $m^2 g^{-1}$. Surface area of CN_A900 is more than twice as high as that of C900. This implies that fluffy material obtained by the combustion of the mixture has yielded the carbon samples of greater surface area than the C samples. In the case of CN_B900, surface area of as high as 518 $m^2 g^{-1}$ is observed. However, surface area of CN_B900 is only 29 $m^2 g^{-1}$ higher than CN_A900, even though the ratio of AN to sucrose used is higher in the case of CN_B900. This implies that after a certain amount of AN, its quantity may not have a considerable effect on surface area of the resulting carbon. The total pore volumes of the all carbon samples lie between 0.01 and 0.32 $cm^3 g^{-1}$. Similar to surface area, pore volumes also increase with the increase in the temperature. These lower pore volumes (< 0.32 $cm^3 g^{-1}$) observed for the materials with high surface areas indicate that the carbon samples are microporous.[50, 51]

Nitrogen adsorption–desorption isotherm, BJH and Horvath-Kawazoe pore size distributions of CN_B900 are provided in Fig. 6. Fig. 6a shows the type I isotherm of IUPAC classification for CN_B900, which is characteristic of microporous material.[52] BJH pore size distribution in the inset of Fig. 6a shows that average pore diameter lies below 2 nm and confirms that CN_B900 is mainly microporous. Horvath-Kawazoe pore size distribution of CN_B900 in Fig. 6b shows the sharp peak centered in the region of micropores show that the average pore width of CN_B900 is 0.5 nm. Also, *t*-plot surface area and the external surface area of CN_B900 are 458 $m^2\ g^{-1}$ and 60 $m^2\ g^{-1}$ respectively. This implies that 88.4 % of the total surface area of CN_B900 is contributed by its micropores. Three dimensionally porous graphene balls obtained from coal tar pitch by KOH activation has shown SSA up to 1947 m^2g^{-1}.[53] An animal cellulose precursor has yielded an O-rich activated carbon with a SSA of 3442 $m^2\ g^{-1}$ with KOH activation.[54] N-carbon nanosheets derived from the *Typha orientalis* plant exhibit a SSA of 1498 $m^2\ g^{-1}$.[43] A bean dregs-derived activated carbon activated with KOH shows a SSA of 2876 $m^2\ g^{-1}$.[55] A sucrose-derived hydrochar, by the activation with steam and KOH, has yielded activated carbons with SSAs of 814 and 2431 $m^2\ g^{-1}$ respectively.[10] According to another report, KOH activation of sucrose-derived carbon spheres yields a carbon with a SSA of 2823 $m^2\ g^{-1}$.[56] A sucrose-derived activated carbon obtained by phosphoric acid activation has been reported to show a SSA of 460 $m^2\ g^{-1}$.[57] A carbon derived from sucrose with $ZnCl_2$ activation shows a SSA of 1434 $m^2\ g^{-1}$.[58] Activated carbons synthesized from sucrose with CO_2 activation show SSA up to 2953 $m^2\ g^{-1}$.[59] These reports imply that KOH and CO_2 activations offer better SSAs for activated carbons obtained from sucrose than the other activation methods.

TG-DTG profiles of C, CN_A and CN_B sample synthesized at 900 °C, performed in air atmosphere are given in Fig. 7. TGA and DTG of C900 indicates that there are three different events of weight loss occurring. According to DTG, those events are centered at 314, 538 and 616 °C and the corresponding weight losses are 8.9, 57.7 and 29.9 %. In the cases of CN_A900 and CN_B900,

only two weight losses are observed and the major weight losses occur at 590 and 597 °C respectively. As for $CN_A900$and CN_B900, the starting point of the major weight loss is 438 and 448 °C respectively and major weight losses are 89.9 and 90.4 % respectively. Their initial steady weight losses occurring up to 438 and 448 °C correspond to 8.4 and 8.3 % respectively. The initial weight loss occurring below 448 °C is due to the removal water molecules and volatile matter present on the carbon.[52, 60] The major weight loss of the carbon occurs due to the burning of the carbon by reacting with oxygen present in the air. The low temperature burning of the C900 happens due to the possession of functional groups and /or its low degree of graphitic nature. Among three samples under study, CN_B900 shows the best thermal stability. The higher thermal stability shown by the CN_A900 and CN_B900 might be due to that they may not possess easily-oxidizable functional groups and/or their high degrees of graphitic nature.[61]

3.6. Electron microscopic studies

SEM images of carbon samples synthesized at 900 °C are given in Fig. 8. SEM images of all carbons show particles of non-spherical morphologies including sheet and of polydispersity. C900 in Fig. 8a shows the particles of size in the range of ~ 250 nm to ~ 9 μm. CN_A900 shows particles of size between ~ 200 nm and ~ 18 μm (Fig. 8b). As for CN_B900 (in Fig. 8c) , the size ranges from ~ 200 nm to ~ 21 μm. SEM analysis reveals that the synthesized carbons are of wide particles size distribution. Similar morphologies for carbons derived from sucrose have already been reported.[9, 59] XRD and SEM analyses prove that the fine carbon crystallites (sheets) are randomly arranged in carbon particles of size in the range of several nanometers to several micrometers. In other words, the carbon particles are polycrystalline in nature.[60] TEM image of CN_B900 shown in Fig. 8d shows the presence of particles of different shapes and sizes. There are several sheet-like particles seen in the TEM. These sheets must be made of several graphene layers. The relatively higher transparency (to electron beam) shown by these sheets is due to their

lower thicknesses and the electrons can penetrate these sheets. In addition to sheets, there are aggregates of small particles whose average size lies below 10 nm.

3.7. Mechanism of formation of carbons

According to ^{13}C NMR and FTIR results, carbons from gummy material and fluffy materials are different in terms of graphitic nature and textural properties. Due to the decomposition of AN after the evaporation of water from the aqueous mixture of sucrose and AN, a lot of heat and gases such as N_2, H_2O, O_2, OH, HNO, NO_3 might evolve. It is because decomposition of AN is exothermic.[23] Charring of sucrose occurs due to the heat generated, and the foamy, voluminous appearance of fluffy precursor is given rise to due to the sudden evolution of gases. There is a possibility that sucrose might react with AN and its decomposition products, which is evident from the presence of nitrogen revealed by CHN elemental and XPS analyses. As for both gummy and fluffy precursors, the carbons are aliphatic in nature. In the case of precursor formed with the use of sucrose alone, caramel, a polymer of sucrose, is only formed.[29, 62] Further, upon carbonization process of both precursors at high temperatures, subsequent polymerization by condensation reactions and aromatization by dehydration and dehydrogenation reactions to form polynuclear aromatic hydrocarbons (PAHs) occur.[8, 63] Subsequently, formation of graphene layers and their ordering (graphitization) to certain extent might take place.[64, 65] In general, the degree of graphitization is found to be low in sucrose-derived carbons even if the treatment temperature is as high as 1400 °C.[62] Steam activation also has been known to favor the graphitization process. [49]

3.8. Electrochemical studies

Cyclic voltammograms (CVs) of carbon samples synthesized at different temperatures were collected in order to understand the nature of the capacitance operating in the case of carbon materials under study. Shape of the CV indicates the nature of the capacitance operating as to whether it is EDLC, pseudocapacitance or both. CVs of C, CN_A and CN_B samples synthesized at 900 °C are given in Fig. 9a and of C and CN_B synthesized at 600 - 800 °C are given in Fig. S1a

and Fig. S2b of supplementary data. The observed shapes of CVs are attributed uniquely to carbon materials, revealing that both EDLC (non-Faradaic) and pseudocapacitance (Faradaic) take roles here.[6, 66] The CVs are not rectangular due to that some redox events taking place in the potential range of 0-0.5 V. These redox reactions occur due to the presence of some functional groups in the carbons.[6] Not only activated carbons but also CNTs and graphenes having functional groups (generated by oxidation with air, acid or by electro oxidation) exhibit this type of CV shape.[66-68] Moreover, carbons having quinonic, phenolic, carboxylic oxygen groups and pyridinic (N-6) and pyrrolic (N-5) nitrogen groups can undergo redox reactions and hence show peaks in their CVs.[12, 69, 70,65] Since the area of the CV is directly proportional to specific capacitance (C_s) of the electrode material, the C_s of the carbons obtained at 900 °C should be in the following order; $CN_B900 > CN_A900 > C900$. For C samples obtained at < 900 °C, the order of Cs should be C800 > C700 > C600. The same should be the order for CN_B samples. However, there is a high degree of decline in the area of the CV for C samples while moving to lower carbonization temperature from 800 °C. Moreover, the areas of CV for C800, C700 and C600 samples are much lower than that of their CN_B analogues.

Charge-discharge curves of the carbon samples collected for estimating specific capacitance are shown in Fig. 9b, Fig. S1b and Fig. S2b. The charge-discharge curves are linear and symmetrical, indicating the ideal capacitive characteristics. As for the plot, CN_B900 and C900 take the longest and the shortest times respectively for charging and discharging, revealing that CN_B900 and C900 hold the highest and the lowest charge-storage capacity among the three sets of carbons synthesized at 900 °C. As for the C and CN_B samples made at 600 - 800 °C, the charging capacity is found to be higher for 800 °C analogues than their low temperature counterparts. Specific capacitance (C_s) of the carbon is calculated from galvanostatic discharge curves using the following relationship. $C_s = I\Delta t/\Delta V m$, where, '$I$' is the current,'$\Delta t$' is discharge time of cycle,

'*ΔV*' is potential window and 'm' is mass of carbon.[4] The C_s values of C900, CN_A900 and CN_B900 are 62, 259, and 277 F g^{-1} respectively. The order of the C_s of the carbons is as follows; $CN_B900 > CN_A900 > C900$. The trend observed among the C_s values of carbons is consistent with their trend with surface areas. The Cs values of CN_A900 and CN_B900 are due to effect of the precursors used. In order to ignore the effect of specific surface area (SSA) and understand the effect of other factors, ratio of C_s and SSA can be considered. The C_s/SSA values for C900, CN_A900 and CN_B900 are 0.30, 0.53 and 0.53 F m^{-2}. The difference of 0.23 F m^{-2} observed between CN_B900 and C900 may be due to the difference in conductivities, functional groups, wettability in electrolyte and diffusion barrier arising from the pore size, among these carbons.[12, 20, 34, 71]

Activated carbon synthesized from sucrose with CO_2 activation at 900 °C for 4 h and having a SSA of 2102 m^2 g^{-1}, showed a C_s value of 165 F g^{-1} in 1 M sulphuric acid (C_s/SSA = 0.08).[59] Activated microporous carbon nanofibers with the surface area of 597 m^2 g^{-1} showed a C_s value of 256 F g^{-1} in 6 M KOH electrolyte (C_s/SSA = 0.43).[51] Activated carbon synthesized from sucrose-derived carbon spheres with a SSA of 2823 m^2 g^{-1} shows a Cs of 316 F g^{-1} in 6 M KOH electrolyte (C_s/SSA = 0.11).[56] This implies that CN_A and CN_B carbons of the current work show superior performances even though they show lower SSAs. The Cs values and Cs/SSA ratio of the C600, C700 and C800 are 2, 3 and 35 F g^{-1} and 0.18, 0.19 and 0.25 F m^{-2} respectively. This reveals that Cs values decrease drastically while reducing the carbonization temperature from 800 °C to lower temperatures. This decrease might be due to the drastic reduction in SSA values. This proves the dependency of capacitance on surface area of the samples. It is worth to note that the Cs/SSA does not reduce considerably like Cs does. CN_B600, CN_B700 and CN_B800 exhibit the Cs values of 18, 124 and 213 F g^{-1} and Cs/SSA of 0.38, 0.39 and 0.45 F m^{-2}, respectively. As for the Cs value of CN_B, it decreases with the decrease in the carbonization temperature. However, Cs/SSA value relatively stays as high as 0.38 F m^{-2} for CN_B600 whereas it is only 0.18 for C600.

The poor Cs/SSA values shown by these C samples are probably due to their lower conductivities owing to the low degree of graphitic nature. This clearly indicates that the use of AN in the synthesis has a great role in the positive features of resulting carbons. Also, there is no considerable difference observed in the amount and nature of the observed the functional groups as per the XPS and CHN results, except for the presence of N functional groups (N-6 and N-Q) in CN_B samples.

Regarding the effect of N content on the capacitance of carbon samples, the effect is not pronounced between CN_A900 and CN_B900. It is because their Cs values are the same (i.e., 0.53 F m^{-2}) while having the N content of 2.3 and 3 % respectively. Among all samples, the sum of N (%) and O (%) contents does not differ considerably. However, Cs/SSA values decrease with the reduction in the carbonization temperature. According to XPS analysis, CN_B900 shows the presence of quinone, phenol and/or ether and chemisorbed oxygen (carboxylic acid) along with pyridinic (N-6) and quaternary (N-Q) nitrogen groups in it. Some reports reveal that besides quinone groups, phenolic, carboxylic, pyridinic (N-6) and pyrrolic (N-5) groups can undergo redox reactions to show pseudocapacitance.[12, 70, 72] Moreover, phenolic, carboxylic and quaternary (N-Q) nitrogen groups can improve the electron transfer and wettability of the electrode.[20, 72] Thus, the presence of hetero atoms in the carbon improves the capacitance. However, it is realized that the high temperature carbonization is primarily important for enhanced capacitance of the carbons synthesized by the current method. In other words, the benefits of functional groups are realized only in the carbons of higher carbonization temperatures.

Stability of the capacitance of carbons obtained at 900 °C studied up to 2000 cycles using galvanostatic charge-discharge curves is given in Fig. 9c. Losses of capacitance of C900, CN_A900 and CN_B900 are 8.2, 9.1 and 7.6 % respectively. The initial loss observed with the carbons might probably due to the loss of some amount of functional groups which are contributing to capacitance in terms of redox reactions. Further losses of capacitance observed might be due to

peeling off of the electrode materials from current collector. The good stability shown by the carbon materials prove that they are promising ones for capacitor application.

4. Conclusions

Nitrogen- and oxygen-containing activated carbons have been synthesized using sucrose and ammonium nitrate. Use of ammonium nitrate has not only caused the nitrogen incorporation in carbon but also the formation of carbons with high surface area. N-content of the carbons has increased with the increase in AN to sucrose ratio. One of the carbons obtained at 900 °C from sucrose and AN of 2:1 wt. ratio retains 3 wt. % of nitrogen in it. The carbons obtained using AN are found to be more graphitic and exhibit greater crystallite size (L_c) than the carbons from sucrose alone. The surface areas of carbons obtained using AN are as high as more than twice as that of carbons from sucrose alone. The steam activation employed here yields the microporous carbons. ^{13}C NMR analysis proved that the carbons derived using AN show only the carbons of aromatic nature whereas non-N-containing carbon shows the presence of carbons with other functionalities including phenol and carbonyl carbons. Thermal stability of the N-containing carbons in air is found to be higher than non-N-containing carbons.

SEM and TEM results show that carbons particles synthesized are of size in the range of several nanometers to several micrometers with irregular shapes and they are proved to be polycrystalline in nature in complementary with XRD results. The presence of some graphene sheets also are identified along with 3 D particles of carbon by TEM imaging. Electrochemical studies indicate the synthesized carbons show EDLC besides pseudocapacitance due to the presence of oxygen and nitrogen functional groups. One of the N- and O-containing carbons with the highest BET surface area of 518 $m^2\ g^{-1}$ shows a specific capacitance of 277 F g^{-1}. Reason for the higher SSA/Cs values shown by N- and O-containing carbons (900 °C) is believed to be due to higher surface area and higher graphitic nature along with the presence of functional groups.

Also, these carbons show excellent stability of capacitance over 2000 cycles. Thus, this synthetic method can be a promising for the synthesis of N- and O-containing carbons and the synthesized N- and O-containing carbons can be potential candidates for supercapacitor application.

Acknowledgements

We acknowledge (Late) Prof. R. P. Viswanath and Prof. T. K. Varadarajan for their contributions to this work. The Department of Science and Technology (Government of India) is thankfully acknowledged for funding NCCR.

Notes and references

1. Y. Zhai, Y. Dou, D. Zhao, P. F. Fulvio, R. T. Mayes and S. Dai, *Adv. Mater.*, 2011, **23**, 4828-4850.
2. J. Yan, Q. Wang, T. Wei and Z. Fan, *Adv. Energy Mater.*, 2014, **4**, 1300816.
3. P. Simon and Y. Gogotsi, *Nat Mater*, 2008, **7**, 845-854.
4. N. Subramanian, B. Viswanathan and T. K. Varadarajan, *RSC Adv.*, 2014, **4**, 33911-33922.
5. M. Inagaki, H. Konno and O. Tanaike, *J. Power Sources*, 2010, **195**, 7880-7903.
6. E. Frackowiak and F. Béguin, *Carbon*, 2001, **39**, 937-950.
7. M. Sevilla and R. Mokaya, *Energy Environ. Sci.*, 2014, **7**, 1250-1280.
8. A. G. Pandolfo and A. F. Hollenkamp, *J. Power Sources*, 2006, **157**, 11-27.
9. L. Wei and G. Yushin, *J. Power Sources*, 2011, **196**, 4072-4079.
10. A. S. Mestre, E. Tyszko, M. A. Andrade, M. Galhetas, C. Freire and A. P. Carvalho, *RSC Adv.*, 2015, **5**, 19696-19707.
11. X. Y. Chen, C. Chen, Z. J. Zhang, D. H. Xie, X. Deng and J. W. Liu, *J. Power Sources*, 2013, **230**, 50-58.
12. H. Liu, H. Song, X. Chen, S. Zhang, J. Zhou and Z. Ma, *J. Power Sources*, 2015, **285**, 303-309.
13. Y. a. Huang, F. Yang, Z. Xu and J. Shen, *J. Colloid Interface Sci.*, 2011, **363**, 193-198.
14. G. Ćirić-Marjanović, I. Pašti, N. Gavrilov, A. Janošević and S. Mentus, *Chem. Pap.*, 2013, **67**, 781-813.
15. T. E. Rufford, D. Hulicova-Jurcakova, Z. Zhu and G. Q. Lu, *Electrochem. Commun.*, 2008, **10**, 1594-1597.
16. A. Bagreev, J. Angel Menendez, I. Dukhno, Y. Tarasenko and T. J. Bandosz, *Carbon*, 2004, **42**, 469-476.
17. T. Horikawa, N. Sakao, T. Sekida, J. i. Hayashi, D. D. Do and M. Katoh, *Carbon*, 2012, **50**, 1833-1842.
18. N. Kan-nari, S. Okamura, S.-i. Fujita, J.-i. Ozaki and M. Arai, *Adv. Synth. Catal.*, 2010, **352**, 1476-1484.
19. P. Pramanik, *Bull. Mater. Sci.*, 1999, **22**, 335-339.
20. D. Hulicova-Jurcakova, M. Seredych, G. Q. Lu and T. J. Bandosz, *Adv. Funct. Mater.*, 2009, **19**, 438-447.
21. K. Okajima, K. Ohta and M. Sudoh, *Electrochim. Acta*, 2005, **50**, 2227-2231.

22. Z. R. Yue, W. Jiang, L. Wang, S. D. Gardner and C. U. Pittman Jr, *Carbon*, 1999, **37**, 1785-1796.
23. S. Cagnina, P. Rotureau, G. Fayet and C. Adamo, *Phys. Chem. Chem. Phys.*, 2013, **15**, 10849-10858.
24. L. Lai, H. Yang, L. Wang, B. K. Teh, J. Zhong, H. Chou, L. Chen, W. Chen, Z. Shen, R. S. Ruoff and J. Lin, *ACS Nano*, 2012, **6**, 5941-5951.
25. C. R. Marcela Guiotoku, Claudia Maia and Dachamir Hotza, in *Microwave Heating*, ed. U. Chandra, InTech, 2011, ch. 13, pp. 291-308.
26. Y.-G. Zhou, J.-J. Chen, F.-b. Wang, Z.-H. Sheng and X.-H. Xia, *Chem. Commun.*, 2010, **46**, 5951-5953.
27. L. Muniandy, F. Adam, A. R. Mohamed and E.-P. Ng, *Microporous Mesoporous Mater.*, 2014, **197**, 316-323.
28. H. Takagi, K. Maruyama, N. Yoshizawa, Y. Yamada and Y. Sato, *Fuel*, 2004, **83**, 2427-2433.
29. M. Darder and E. Ruiz-Hitzky, *J Mater. Chem.*, 2005, **15**, 3913-3918.
30. A. M. Vassallo and R. Codd, *Carbon*, 1988, **26**, 553-558.
31. T. E. McGrath, W. G. Chan and M. R. Hajaligol, *J. Anal. Appl. Pyrolysis*, 2003, **66**, 51-70.
32. A. B. Brizuela, L. C. Bichara, E. Romano, A. Yurquina, S. Locatelli and S. A. Brandán, *Carbohydr. Res.*, 2012, **361**, 212-218.
33. H. K. Sadhanala, J. Khatei and K. K. Nanda, *RSC Adv.*, 2014, **4**, 11481-11485.
34. M. Seredych, D. Hulicova-Jurcakova, G. Q. Lu and T. J. Bandosz, *Carbon*, 2008, **46**, 1475-1488.
35. Y. Guo and D. A. Rockstraw, *Carbon*, 2006, **44**, 1464-1475.
36. J. Zawadzki, *Carbon*, 1995, **33**, 1541-1546.
37. M.-W. Jung, K.-H. Ahn, Y. Lee, K.-P. Kim, J.-S. Rhee, J. Tae Park and K.-J. Paeng, *Microchem. J.*, 2001, **70**, 123-131.
38. J. P. de Celis, M. S. Villaverde, A. L. Cukierman and N. E. Amadeo, *Lat. Am. Appl. Res.*, 2009, **39**, 165-171.
39. M. Sevilla and A. B. Fuertes, *Carbon*, 2009, **47**, 2281-2289.
40. S. Biniak, G. Szymanski, J. Siedlewski and A. Swiatkowski, *Carbon*, 1997, **35**, 1799-1810.
41. Z. Yue, J. Economy and G. Bordson, *J Mater. Chem.*, 2006, **16**, 1456-1461.
42. A. M. Puziy, O. I. Poddubnaya, R. P. Socha, J. Gurgul and M. Wisniewski, *Carbon*, 2008, **46**, 2113-2123.
43. P. Chen, L.-K. Wang, G. Wang, M.-R. Gao, J. Ge, W.-J. Yuan, Y.-H. Shen, A.-J. Xie and S.-H. Yu, *Energy Environ. Sci.*, 2014, **7**, 4095-4103.
44. A. J. Plomp, D. S. Su, K. P. d. Jong and J. H. Bitter, *J Phys. Chem. C*, 2009, **113**, 9865-9869.
45. D. Lennon, D. T. Lundie, S. D. Jackson, G. J. Kelly and S. F. Parker, *Langmuir*, 2002, **18**, 4667-4673.
46. M. Kim, S. Hwang and J.-S. Yu, *J Mater. Chem.*, 2007, **17**, 1656-1659.
47. Y. Zhang, Z. Schnepp, J. Cao, S. Ouyang, Y. Li, J. Ye and S. Liu, *Sci. Rep.*, 2013, **3**.
48. T. Susi, T. Pichler and P. Ayala, *Beilstein J Nanotech.*, 2015, **6**, 177-192.
49. K. László, E. Tombácz and K. Josepovits, *Carbon*, 2001, **39**, 1217-1228.

50. Y. J. Kim, Y. Abe, T. Yanagiura, K. C. Park, M. Shimizu, T. Iwazaki, S. Nakagawa, M. Endo and M. S. Dresselhaus, *Carbon*, 2007, **45**, 2116-2125.
51. C. Ma, Y. Song, J. Shi, D. Zhang, X. Zhai, M. Zhong, Q. Guo and L. Liu, *Carbon*, 2013, **51**, 290-300.
52. Z. Hu, M. P. Srinivasan and Y. Ni, *Carbon*, 2001, **39**, 877-886.
53. X. He, H. Zhang, H. Zhang, X. Li, N. Xiao and J. Qiu, *J Mater. Chem. A*, 2014, **2**, 19633-19640.
54. Y. Gao, Q. Yue and B. Gao, *RSC Adv.*, 2015, **5**, 31375-31383.
55. C. Ruan, K. Ai and L. Lu, *RSC Adv.*, 2014, **4**, 30887-30895.
56. L. Mao, Y. Zhang, Y. Hu, K. H. Ho, Q. Ke, H. Liu, Z. Hu, D. Zhao and J. Wang, *RSC Adv.*, 2015, **5**, 9307-9313.
57. H. Liu, J. Zhang, H. H. Ngo, W. Guo, H. Wu, C. Cheng, Z. Guo and C. Zhang, *RSC Adv.*, 2015, **5**, 52048-52056.
58. T. E. Rufford, E. Fiset, D. Hulicova-Jurcakova and Z. Zhu, in *Green Carbon Materials: Advances and Applications*, eds. T. E. Rufford, J. Zhu and D. Hulicova-Jurcakova, CRC press, Boca Raton, 2014, ch. 4, pp. 93-113.
59. L. Wei and G. Yushin, *Carbon*, 2011, **49**, 4830-4838.
60. J. Kong, Q. Yue, B. Wang, L. Huang, B. Gao, Y. Wang and Q. Li, *J. Anal. Appl. Pyrolysis*, 2013, **104**, 710-713.
61. T.-W. Kim, I.-S. Park and R. Ryoo, *Angew. Chem.*, 2003, **115**, 4511-4515.
62. E. R. Buiel, A. E. George and J. R. Dahn, *Carbon*, 1999, **37**, 1399-1407.
63. H. Marsh, M. Martínez-Escandell and F. Rodríguez-Reinoso, *Carbon*, 1999, **37**, 363-390.
64. M. Sevilla and A. B. Fuertes, *Chem. - Eur. J.*, 2009, **15**, 4195-4203.
65. P. Adelhelm and P. E. de Jongh, *J Mater. Chem.*, 2011, **21**, 2417-2427.
66. R. Wang and X. Yan, *Sci. Rep.*, 2014, **4**.
67. H. Jiang, T. Zhao, C. Li and J. Ma, *Chem. Commun.*, 2011, **47**, 8590-8592.
68. J. H. Chen, W. Z. Li, D. Z. Wang, S. X. Yang, J. G. Wen and Z. F. Ren, *Carbon*, 2002, **40**, 1193-1197.
69. N. P. Wickramaratne, J. Xu, M. Wang, L. Zhu, L. Dai and M. Jaroniec, *Chem. Mater.*, 2014, **26**, 2820-2828.
70. Z. Zhou, Z. Zhang, H. Peng, Y. Qin, G. Li and K. Chen, *RSC Adv.*, 2014, **4**, 5524-5530.
71. L. L. Zhang, Z. Lei, J. Zhang, X. Tian and X. S. Zhao, in *Encycl. Inorg. Chem.*, John Wiley & Sons, Ltd, 2006.
72. C. Yuan, X. Liu, M. Jia, Z. Luo and J. Yao, *J Mater. Chem. A*, 2015, **3**, 3409-3415.

Table

Table 1 Yield, inter planar distance, crystallite size, average number of layers, elemental composition and textural properties of carbon samples

Sample	Yield (%)	$d_{(002)}$ (Å)	L_c (Å)	N_c	C (%)	H (%)	N (%)	O (%)	BET surface area (SSA) ($m^2 g^{-1}$)	Total pore volume ($cm^3 g^{-1}$)
C600	84.2	3.92	5.96	1.52	73.5	3.7	0	22.8	11	0.01
C700	81.4	3.92	5.73	1.46	80.1	2.4	0	17.5	16	0.03
C800	77.4	3.71	7.25	1.95	78.8	2.2	0	19	138	0.11
C900	75.1	3.71	7.42	2.00	77.2	2.4	0	20.4	205	0.13
CN_A600	68.2	3.66	7.40	2.02	78.5	2.3	7.1	12.1	105	0.07
CN_A700	65.0	3.64	7.81	2.15	77.5	2.0	5.6	14.9	277	0.21
CN_A800	61.1	3.59	9.38	2.61	79.0	2.0	4.0	15	370	0.22
CN_A900	58.4	3.54	8.80	2.49	74.4	2.3	2.3	21	489	0.32
CN_B600	63.6	3.66	7.60	2.07	75.7	2.3	8.8	13.2	47	0.06
CN_B700	59.2	3.59	8.52	2.38	77.7	2.0	7.1	13.2	320	0.18
CN_B800	56.8	3.50	9.72	2.78	76.5	2.0	4.1	17.4	477	0.25
CN_B900	53.7	3.50	9.09	2.60	74.6	2.0	3.0	20.4	518	0.28

List of figures captions

Fig. 1 Photograph of precursors used for the synthesis of C and CN_B carbon samples. The precursors were obtained from aqueous sucrose (C) and aqueous mixture of sucrose and ammonium nitrate (CN_B).

Fig. 2 Powder XRD patterns of carbon samples synthesized at different temperatures.

Fig. 3 Solid-state ^{13}C NMR spectra of carbon samples synthesized at 800 °C, fluffy material and sucrose.

Fig. 4 FTIR spectra of carbon samples synthesized at different temperatures.

Fig. 5 XPS of C900 and CN_B900 samples. C1s and O1s core level spectra of C900 and C1s, N1s and O1s core level spectra of CN_B900.

Fig. 6 Nitrogen adsorption-desorption isotherm (a), BJH pore size distribution (inset of a) and Horvath-Kawazoe pore size distribution (b) of CN_B900.

Fig. 7 TG-DTG profiles of carbon samples synthesized at 900 °C, recorded in air atmosphere.

Fig. 8 SEM images of C900 (a), CN_A900 (b) and CN_B900 (c) and TEM image of CN_B900 (d).

Fig. 9 (a) Cyclic voltammograms of carbons, recorded in 1 M H_2SO_4 at the scan rate of 10 mV s^{-1} , (b) galvanostatic charge-discharge curves collected with a current of 0.5 mA and (c) plot of variation of specific capacitance with cycle number of galvanostatic charge-discharge.

Figures

Fig. 1 Photograph of precursors used for the synthesis of C and CN_B carbon samples. The precursors were obtained from aqueous sucrose (C) and aqueous mixture of sucrose and ammonium nitrate (CN_B).

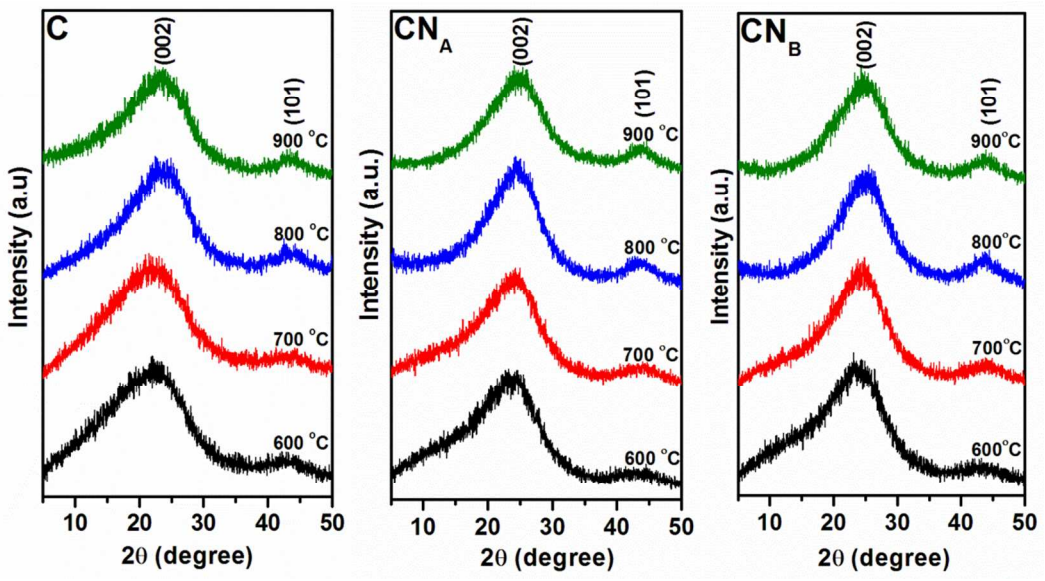

Fig. 2 Powder XRD patterns of carbon samples synthesized at different temperatures.

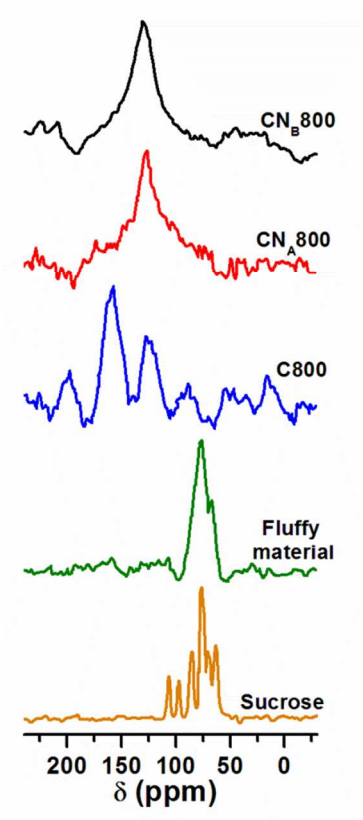

Fig. 3 Solid-state ^{13}C NMR spectra of carbon samples synthesized at 800 °C, fluffy material and sucrose.

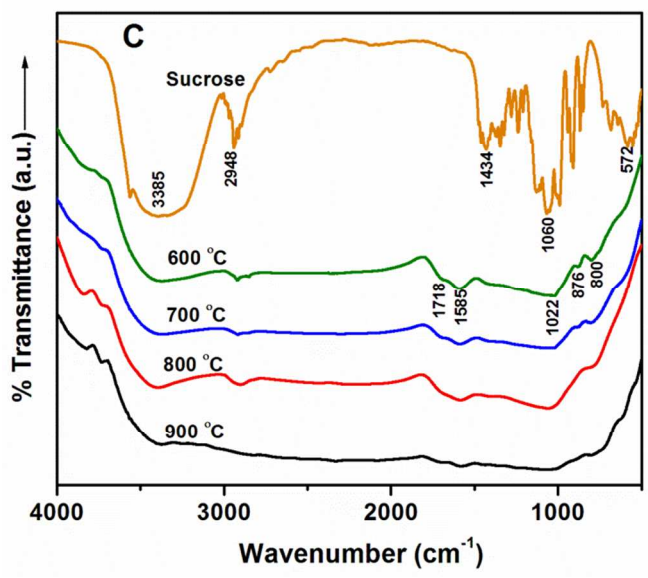

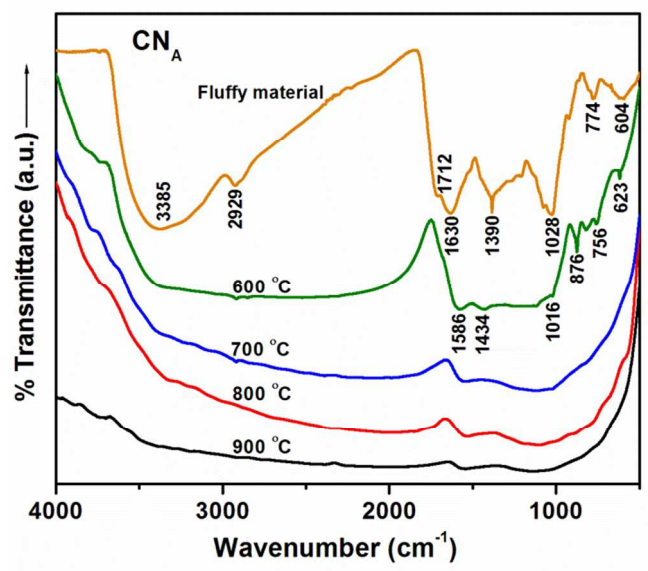

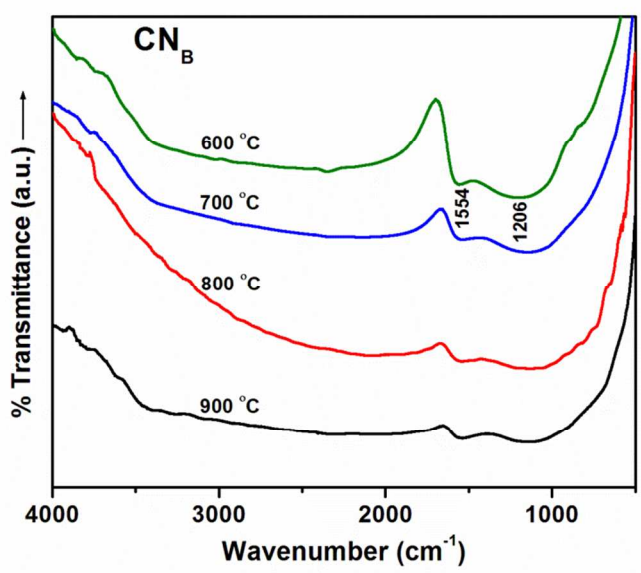

Fig. 4 FTIR spectra of carbon samples synthesized at different temperatures.

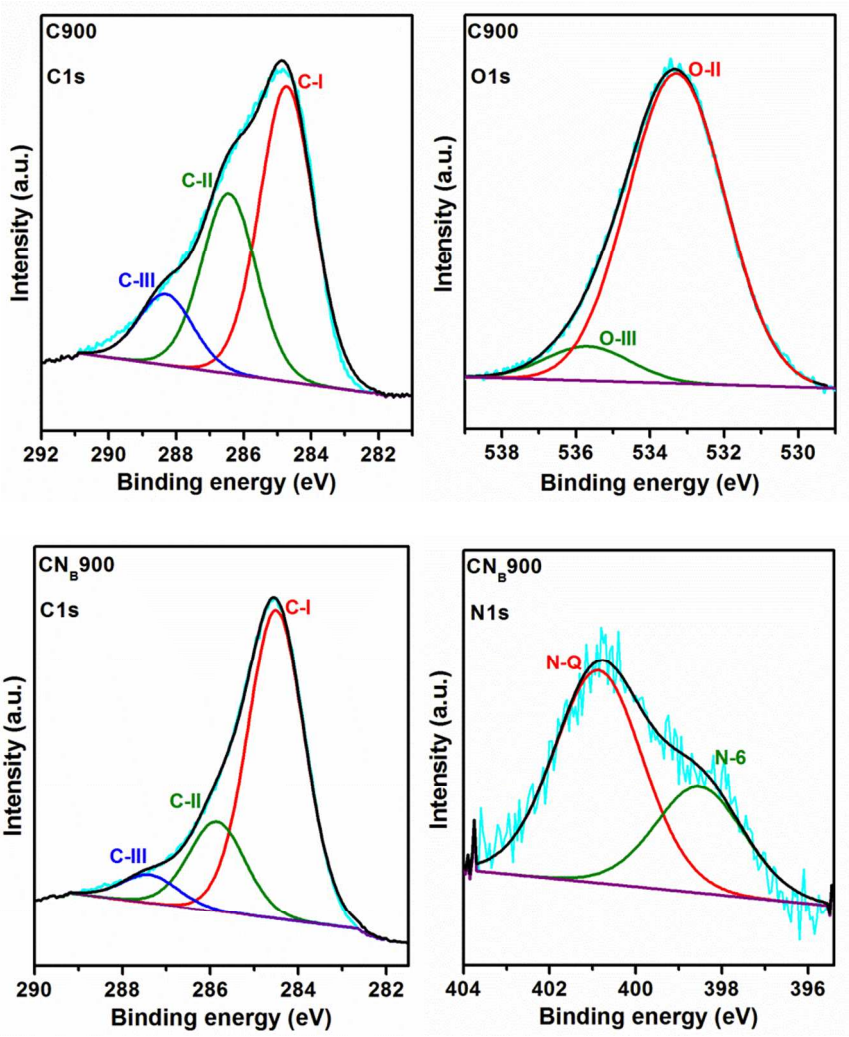

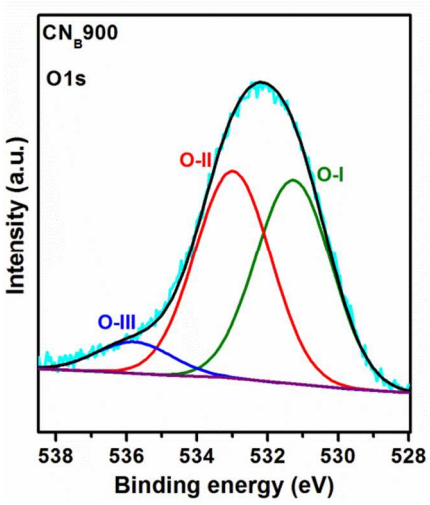

Fig. 5 XPS of C900 and CN_B900 samples. C1s and O1s core level spectra of C900 and C1s, N1s and O1s core level spectra of CN_B900

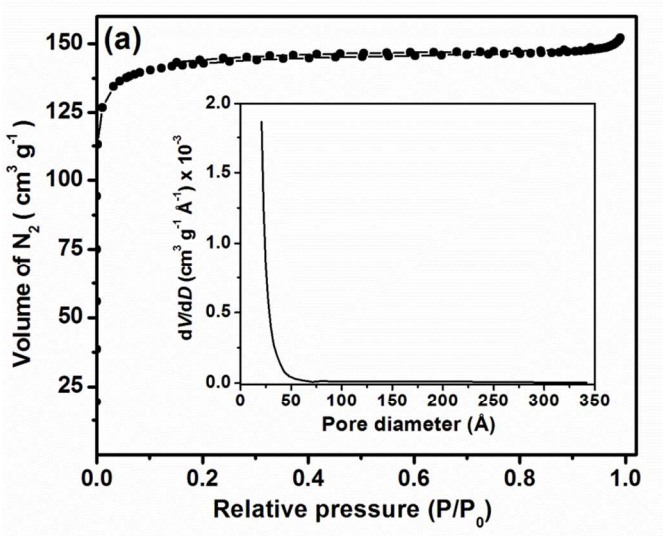

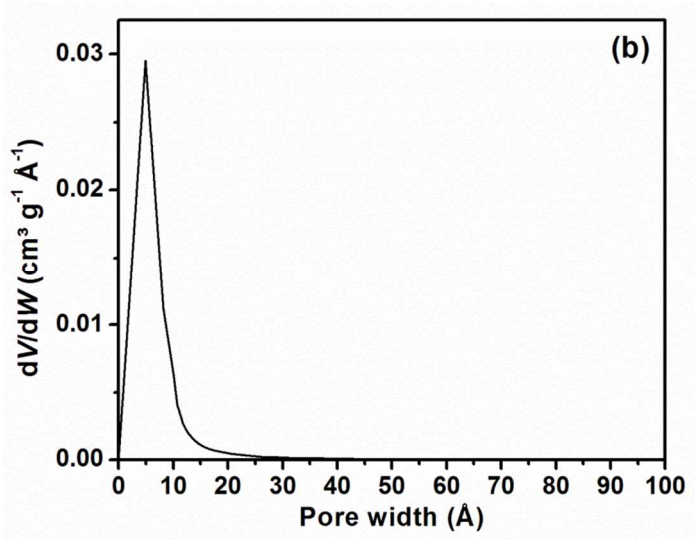

Fig. 6 Nitrogen adsorption-desorption isotherm (a), BJH pore size distribution (inset of a) and Horvath-Kawazoe pore size distribution (b) of CN_B900

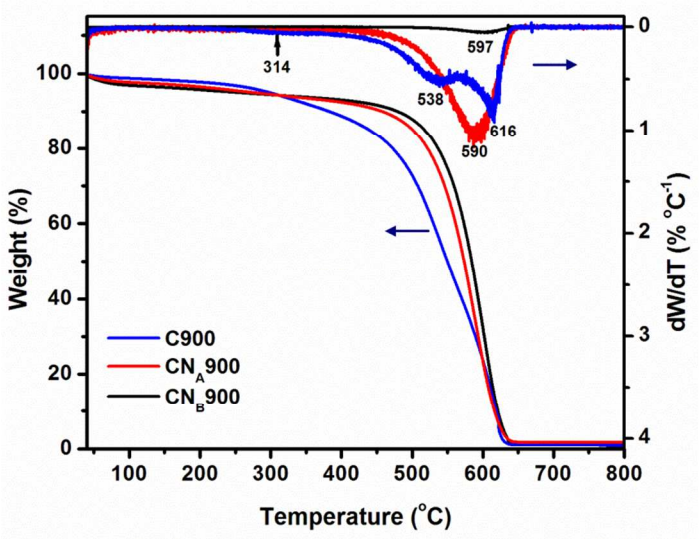

Fig. 7 TG-DTG profiles of carbon samples synthesized at 900 °C, recorded in air atmosphere.

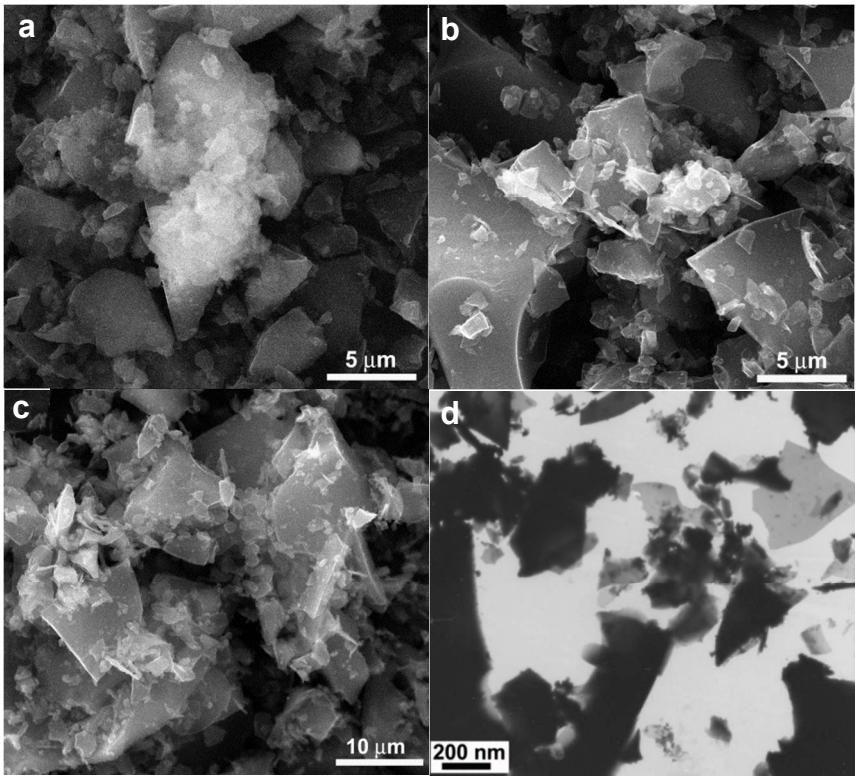

Fig. 8 SEM images of C900 (a), CN_A900 (b) and CN_B900 (c) and TEM image of CN_B900 (d).

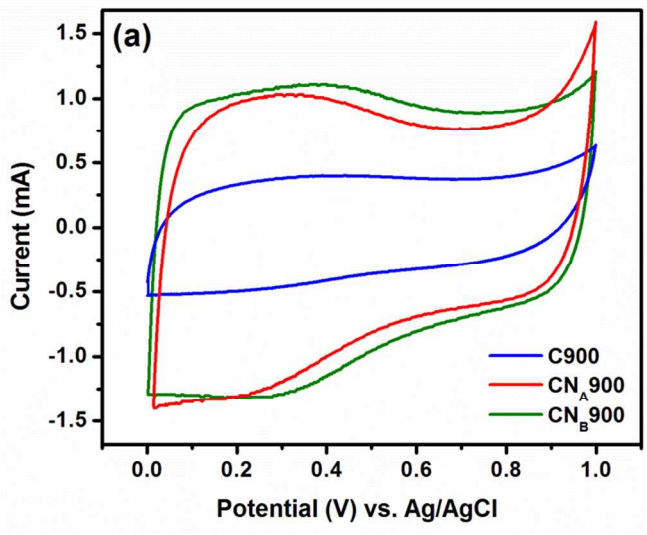

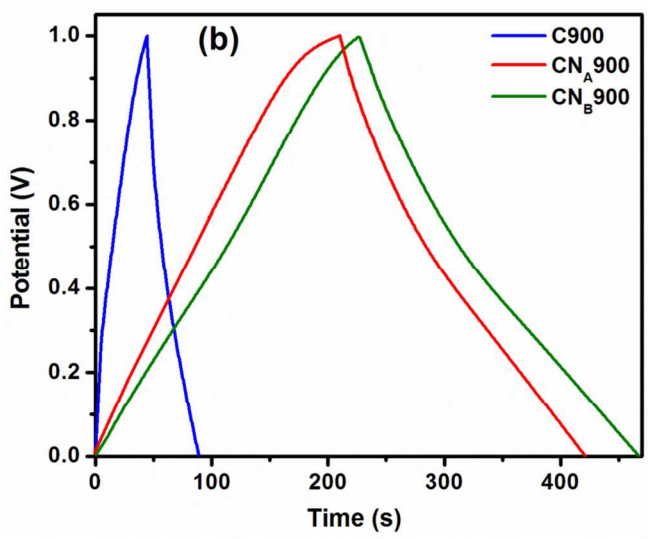

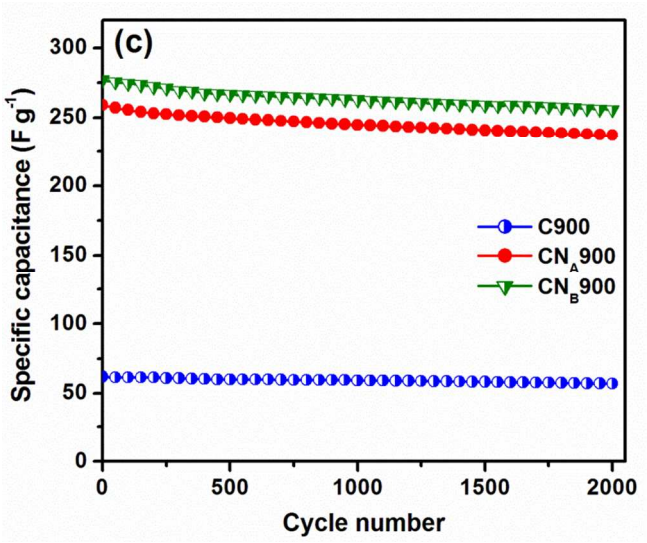

Fig. 9 (a) Cyclic voltammograms of carbons, recorded in 1 M H_2SO_4 at the scan rate of 10 mV s^{-1} , (b) galvanostatic charge-discharge curves collected with a current of 0.5 mA and (c) plot of variation of specific capacitance with cycle number of galvanostatic charge-discharge.